VOL. 15, NO. 22, NOVEMBER 2020 ISSN 1819-6608
ARPN Journal of Engineering and Applied Sciences

www.arpnjournals.com

INVESTIGATION OF AERODYNAMIC CHARACTERISTICS OF A WIND-DRIVEN POWER PLANT

A.B. Kabanbayev[1], S.A. Orynbayev[2] and M. Bekmuratov[2]
[1]Karaganda State Technical University, Kazakhstan
[2]Taraz State University after M.Kh. Dulaty, Kazakhstan
E-Mail: seitzhan_74@mail.ru

ABSTRACT

From geographical and meteorological point of view, Kazakhstan is a favorable country for the use of wind energy, the prospects for the use of which are determined by the availability of appropriate wind energy resources. About 50% of the territory of Kazakhstan has an average annual wind speed of 4-5 m/s, and a number of regions have a wind speed of 6 m/s or more, which predetermines good opportunities for using wind energy. The Concept of transition of the Republic of Kazakhstan to sustainable development for 2007-2024 years suggests that the share of alternative energy sources should be 5% in the country's total energy balance by 2024 [1]. The wind energy is considered not only as an ecologically "clean" source of energy - the wind energy also supports socio-economic development, energy security and reduces the dependence of electricity on fuel prices. Currently, the most widespread are turbine wind power plants, the working body of which are turbine rotor blades moving under the action of lifting forces. It is known that turbine wind power plants have a number of disadvantages, including low efficiency [2]. Another type of wind power plant is a wind power plant with a sail in the form of a toroidal shape with an aerodynamic profile. The aim of this work is to study the characteristics of a wind power plant with a blade in the form of a toroidal shape in an aerodynamic tube.

Keywords: aerodynamic tube, lifting force, front resistance, wind speed, impinging angle.

INTRODUCTION

The aerodynamic experiment has now achieved great perfection. The methods used for its implementation are very diverse and can be divided into two groups [3-7]:

- methods in which medium is stationary and body moves;
- methods in which body is stationary, and medium moves.

Each of these groups includes a number of experimental ways of obtaining the relative motion of body and medium. The first group includes the following methods of obtaining the relative motion of body and medium:

- rectilinear motion of body (body dropping, flight tests);
- curvilinear motion of body.

The second group includes:
- use of natural wind;
- aerodynamic tubes.

The experiments in the aerodynamic tube are based on the principle of reversibility of motion, according to which the body motion relative to the air (or liquid) can be replaced by the air motion impinging on a stationary body. To simulate the body motion in the air at rest, it is necessary to create in the aerodynamic tube a uniform flow, which has equal and parallel speeds (uniform speed field), the same density and temperature at any points. Usually in the aerodynamic tube, the flow around a model of a projected object or its parts is investigated and the forces acting on it are determined [8-10]. In this case, it is necessary to observe conditions that provide the ability to transfer the results obtained for the model in the laboratory conditions to a full-sized object. Under these conditions, the aerodynamic coefficients for the studied model and the full-scale object are equal, which allows to determine the aerodynamic coefficient in the aerodynamic tube and calculate the force acting on the nature.

RESEARCH

In the present work, a series of experiments was carried out and analyzed in the aerodynamic tube. All experimental studies were carried out in the laboratory "Aerodynamic measurements" in Ye. A. Buketov Karaganda State University (Kazakhstan) on the aerodynamic tube T-1-M. The test body was stationary. A front resistance force and lifting force of the wind power plant were measured on aerodynamic scales located in the same laboratory.

Figure-1 shows a schematic diagram of the aerodynamic tube T-1-M.

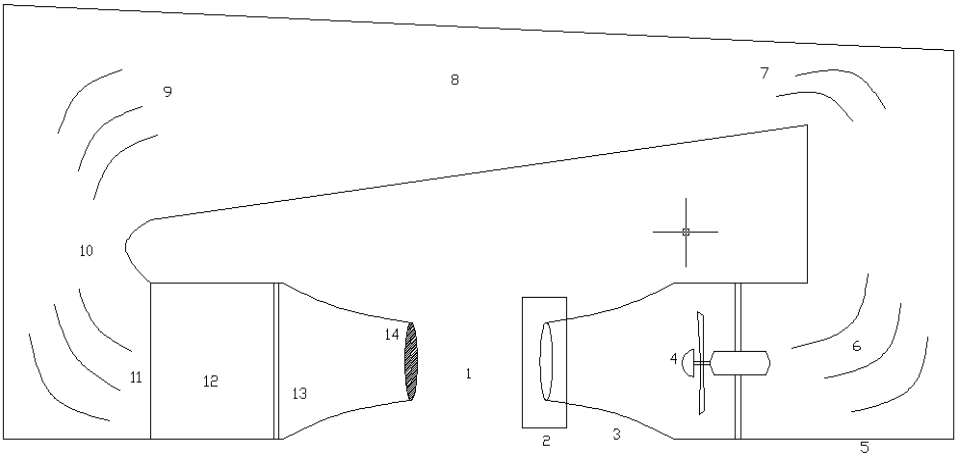

Figure-1. Aerodynamic tube T-1-M diagram:
1 - experiment chamber, 2 - ring, 3 - diffuser, 4 - fan, 5 - transition duct,
6, 7, 9, 10 - turning blades, 8 - return channel, 11-13 - field mesh,
12 - settling chamber, 14 - contraction (nozzle).

Figure-2 shows a photo of the aerodynamic tube T-1-M.

Figure-2. Aerodynamic tube T-1-M.

The model under study is mounted on a frame using racks or extensions; there is also a mechanism for remotely changing the model installation angles [4].
.

Figure-3 shows a diagram of a three-component aerodynamic scale used in the research of this work

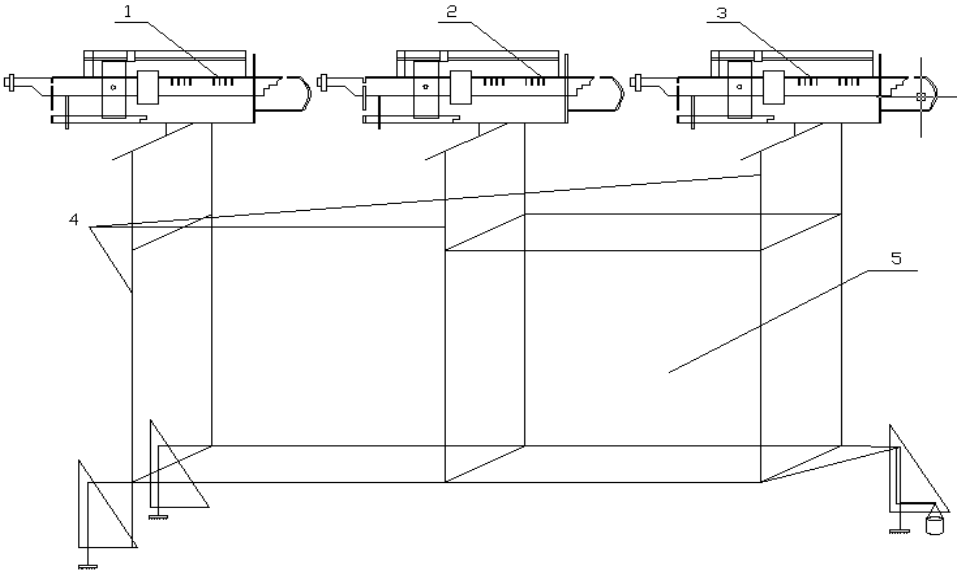

Figure-3. Three-component aerodynamic scales diagram:
1 - scales measuring the front resistance force; 2 and 3 - scales measuring the lifting force; 4 - supports connecting the scales with the experiment chamber; 5 - experiment chamber for installation of the studied models.

Figure-4 shows a general view of the three-component aerodynamic scales

Figure-4. Appearance of the three-component aerodynamic scales.

The main requirement for the three-component aerodynamic scales is independence of measurements on different channels, i.e. so that each weight element measures only the component of the force or moment and does not react to the action of other components.

The three-component aerodynamic scales measure the lifting force and the front resistance force at different flow speeds. The method of attaching these aerodynamic scales is carried out using a thread support (threads, wires) pulled by means of auxiliary weights. The air flow running onto the frontal part of the cylinder exerts force. This force is reflected on the scales. The measurement error of aerodynamic forces and their moments on mechanical aerodynamic scales is 2-3%.

Based on the above, the aerodynamic tube gives the opportunity to determine the aerodynamic characteristics of the toroidal sail of the investigated wind power plant in a full-scale experiment [6]. The sail is made of foam plastic and processed to obtain a smooth surface to improve aerodynamic performance. During the experiment, three sails of the same type with different diameters (40, 45 and 50 cm) were studied.

To determine the energy characteristics of the wind power plant with a sail, the following components of the work of the wind power plant are considered: the sail and manipulator dynamics; forces acting on the sail and their analysis; the possibility of using the manipulator of SHOLKOR robot for the primary conversion of air mass energy; a description of the service model of the wind-driven power plant is given [6].

Figure-5 shows the wind flow effect at a speed of v [m/s] on a toroidal shape hollow body. As a result, the lifting force F_y [N] arises, and the body can be considered as a body with an aerodynamic cross-section profile (sail). At the moment when the air meets the sail, the air flows around the sail from above and below. Due to the sail profile, the air flow around it from below has a lower speed than from above. According to the Bernoulli's law, the higher the flow speed, the lower the pressure in it and vice versa. As a result, when moving in the air flow above the wing, the pressure is less than under it. Due to this difference, the lifting force arises. It pushes out the wing of the plane and, accordingly, the profile itself up. The higher the speed, the greater the lifting force. When the profile is in a horizontal position, the lifting force is equal

to the profile weight. If the profile is located at an angle to the flow (which most often happens), then the angle is called the impinging angle. The impinging angle plays a large role in the formation of the sail's lifting force.

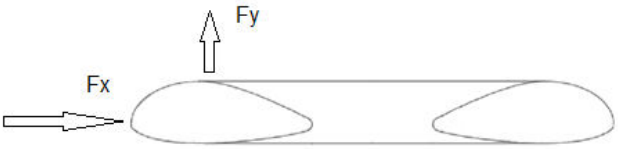

Figure-5. Toroidal hollow body with aerodynamic cross-section profile (sail), Fx - front resistance, and Fy - lifting force.

An experimental model of the wind power plant with a sailing working body, which is a toroidal shape hollow body, was developed and created [7]. Figure-6 shows the experimental model of the wind power plant with a sailing working body.

Figure-6. Experimental model of the wind power plant with a sailing working body:
1 - stationary lower platform, 2 - cylinder rod, 3 - electric generator, 4 - manipulator converter, 5 - sail, 6 - microammeter.

The manipulator converter (manipulator) in the model (Figure-6) operates by using the inverse effect: the upper platform with a sail moves together with the air mass and sets in motion telescopic joints that create translational movements to generate electrical energy [8]. The principle of operation of the wind power plant: the working body of the power plant, the sail 5, is rigidly fixed to the movable platform 4 of the manipulator. A rotor of a linear electric generator 3, generating electric current, is connected to each rod of the telescopic joint (cylinder rod) 2. Thus, the sail captures the kinetic energy of the air mass, and the manipulator converts this energy into mechanical energy of the gradual movements of six rods relative to the cylinders [11-15]. The platform with the sail returns to its original position after the wind flow under the action of elastic bodies or compressed air. Further, the mechanical energy of translational movements by known methods is converted into electrical energy. Microammeters 6 are used in the model to record electric current.

The lifting force (F_y) and the resisting force (F_x) for the aerodynamic profile bodies are determined by the dependencies [12]:

$$Fy = c_A \cdot \frac{1}{2} \cdot \rho \cdot S_P \cdot v_W^2 , \quad (1)$$

$$Fx = c_W \cdot \frac{1}{2} \cdot \rho \cdot S_P \cdot v_W^2 ,$$

where

c_A - experimentally determined coefficient of the lifting force;
c_W - coefficient of the sail's front resistance force;
ρ - air density, kg/m^3;
S_P - area the windy surface, m^2;
v_W - average wind speed, m/s.

The initial for determining the sail size at the initial stage is the required capacity of the wind power plant (N), the approximate value of the wind power plant efficiency (η), as well as the average wind speed in the region where the wind power plant is used (v_W). The energy power of the air mass will be determined by the expression [13]:

$$N_W = \frac{1}{2} \rho \cdot S \cdot v_W^3 , \quad (2)$$

where $N_W = N/\eta$. The efficiency of the wind power plant with the sailing working body is 40%.

The expression (2) determines the frontal surface area, affecting the sail size:

$$S = \frac{2N}{\eta \cdot \rho \cdot v_W^3} . \quad (3)$$

EXPERIMENTAL RESULTS

A series of experiments was carried out with the sail on the aerodynamic tube T-1-M at different wind speeds, but the same impinging angle - 0 degrees. The results of experiments and calculations are summarized in Tables 1-3.

Table-1. Examination of sail Ø 40 cm.

Expe-riment number	Wind speed, m/s	Angle of attack, degrees	Lifting force, F_y, N	Frontal resistan-ce, F_x, N
1	3	0	0.35	1.5
2	5	0	0.7	2
3	8	0	1.35	4.5
4	10	0	2.1	8
5	15	0	4.8	14.3
6	20	0	7.5	25.5

Table-2. Examination of sail Ø 45 cm.

Expe-riment number	Wind speed, m/s	Angle of attack, degrees	Lifting force, F_y, N	Frontal resistance, F_x, N
1	3	0	0.4	2
2	5	0	0,8	2.6
3	8	0	1.5	4.8
4	10	0	2.6	8.8
5	15	0	5.4	16,7
6	20	0	8.75	26.6

Table-3. Examination of sail Ø 50 cm.

Expe-riment number	Wind speed, m/s	Angle of attack, degrees	Lifting force, F_y, N	Frontal resistance, F_x, N
1	3	0	0.5	2.1
2	5	0	0.9	3.2
3	8	0	1.6	8.1
4	10	0	3	10.3
5	15	0	6	19.9

Based on the tabular data, the dependencies of the lifting force F_y on the wind speed for the sail with diameters of 40 cm, 45 cm and 50 cm are constructed at the impinging angle of 0 degrees (Figure-7).

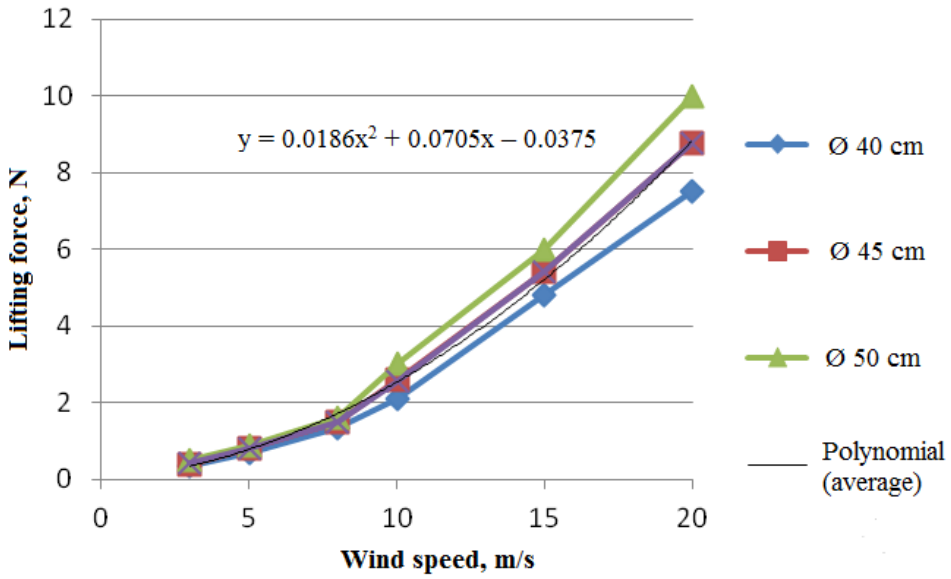

Figure-7. Dependence of the lifting force on the wind speed for the sail with diameters of 40 cm, 45 cm and 50 cm at the impinging angle of 0 degrees.

The lifting force F_y is approximated by the power dependence correlating with the equation (1):

$$y = 0.0186x^2 + 0.0705x - 0.0375, \quad (4)$$

where x - wind speed, m/s.

The graph in Figure-7 shows the change in the lifting sail force from the wind speed and the sail diameter: as the wind speed increases, the lifting force increases in a quadratic manner.

Based on the graph, with high winds, the lifting force increases with a larger sail of the wind power plant and, consequently, the generation of electric energy increases.

Figure-8 shows the dependencies of the front resistance force F_x on the wind speed for the sail with diameters of 40 cm, 45 cm and 50 cm, with the impinging angle of 0 degrees.

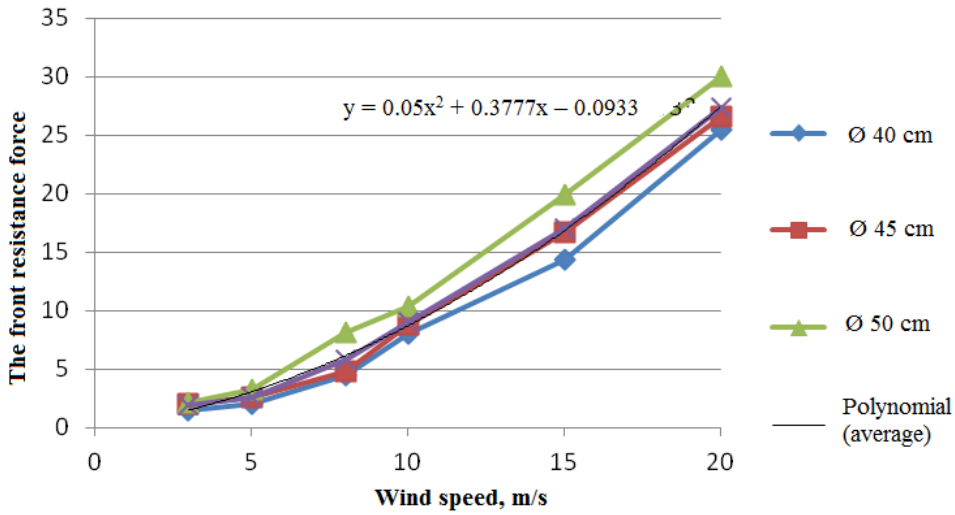

Figure-8. Dependence of the front resistance force on the wind speed for the sail with diameters of 40 cm, 45 cm and 50 cm at the impinging angle of 0 degrees.

The front resistance force F_x is approximated by the power dependence correlating with the equation (1):

$$y = 0.05x^2 + 0.3777x - 0.0933, \quad (5)$$

where x - wind speed, m/s.

The graph in Figure-8 shows how the front resistance of the sail of different diameters varies with increase in the wind speed: the higher the wind speed, the

greater the front resistance. If take the graphs in Figures 7 and 8, then both the front resistance and the lifting force of the sail are directly proportional to the wind speed, given that the impinging angle is 0 degrees.

According to the available data, using the equation (2), the dependencies of the change in the wind power plant capacity on the wind speed for the sail of 40 cm, 45 cm, and 50 cm diameters, with the impinging angle of 0 degrees, are constructed (Figure-9).

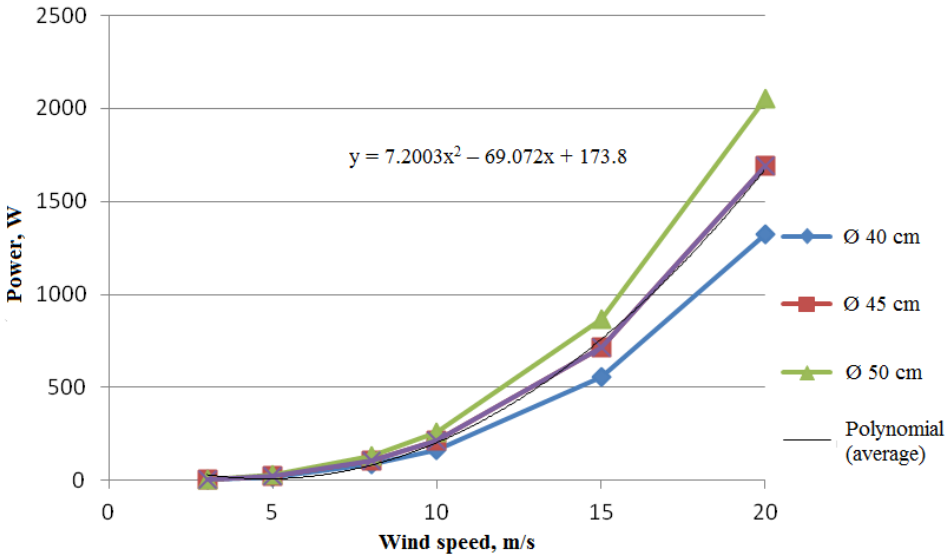

Figure-9. Dependence of the capacity of the wind speed for the sail of 40 cm, 45 cm, and 50 cm diameters.

The wind power plant's capacity is approximated by the power dependence:

$$y = 7.2003x^2 - 69.072x + 173.8, \quad (6)$$

where x - wind speed, m/s.

Based on the data in Figure-9, using the Microsoft Excel prediction feature, the capacity of the wind power plant with the sailing working body for the sail diameter of 25 to 200 cm is calculated and the calculations are summarized in Table-4.

Table-4. Capacity of the wind power plant [W] at the sail diameter of 25 to 200 cm.

Wind speed, m/s	Sail diameter, cm							
	25	**50**	**75**	**100**	**125**	**150**	**175**	**200**
3	0.67	6.90	13.17	19.42	25.67	31.92	38.17	44.42
5	1.89	32.07	62.22	92.38	122.54	152.70	182.87	213.03
8	15.29	131.33	247.59	363.74	479.89	596.04	712.19	828.34
10	29.85	256.52	483.60	710.47	937.35	1164.22	1391.10	1617.97
15	101.11	865.52	1631.36	2396.49	3161.61	3926.74	4691.86	5456.99
20	238.77	2052.16	3868.77	5683.77	7498.77	9313.77	11128.77	12943.77

Based on the data on the average wind speed in the considered area of the wind power plant installation, when varying the diameter of the sail of a mobile wind power plant with the toroidal shape blade with the aerodynamic section profile, the data in Table-4 can be used to determine the estimated generated capacity of the wind power plant.

CONCLUSIONS

The alternative scheme of the wind power plant is proposed. Experimental evidence of the proposed scheme operability is obtained. Mathematical formulas are calculated for the lifting force, the resisting force and capacity depending on the wind speed. Reference tables are compiled to determine the required capacity for generating electric energy, depending on the wind speed and the sail shape. Analysis of the graphs shows that a large sail will give more capacity than a small-diameter sail. As a result of the study of the sail shape and size influence on the received capacity value, it was found that for sails of small diameter it is preferable to work with a larger average wind speed than for sails of large diameter.

This is due to the occurrence of a separation phenomenon at smaller impinging angles than in sails of large diameter. There is a flow separation at positive impinging angles at high speeds, due to the toroid profile asymmetry. In all cases of flow separation, it occurs at the wind speeds above 5 m/s with the exception of a toroid with 400 mm diameter. The toroid with 400 mm diameter has the greatest resistance to the flow separation occurrence at the outlet edge. In terms of creating oscillatory motion at low speeds, it is preferable to use toroids with large diameters at the impinging angles of more than 10-15 degrees, when the lifting force is maximum. If it is necessary to create oscillations in strong winds, then it is better to use a toroid with a small diameter at the impinging angles of 15-20 degrees, which also corresponds to the maximum lifting force, for reasons of permissible oscillation ranges without destroying the plant installation.

REFERENCES

[1] Alibek Nurimbetov, Amangeldy Bekbayev, Seitzhan Orynbayev, Birzhan Baibutanov, Issakul Tumanov, Meruyert Keikimanova. 2015. Optimization of windmill's layered composite Blades to reduce Aerodynamic Noise and Use in Construction of "Green" Cities. Procedia Engineering. 117: 273-287.

[2] Ferhat Kurtulmus, Ali Vardar and Nazmi Izli. 2007. Aerodynamic Analyses of Different Wind Turbine Blade Profiles. Journal of Applied Sciences. 7: 663-670.

[3] N. Thouault, C. Breitsamter, N. A. Adams, C. Gologan, J. Seifert. 2009. Experimental investigation of the aerodynamic characteristics of generic fan-in-wing configurations. The Aeronautical Journal. 113(1139): 9-20.

[4] L.I. Garipova, A.S. Batrakov, A.N. Kusyumov, S.A. Mikhailov, G.N. Barakos. 2014. Estimates of hover aerodynamics performance of rotor model. Russian Aeronautics (Iz VUZ). 57(3): 223-231.

[5] Nik Ahmad Ridhwan Nik Mohd and G.N. Barakos, 2012. Computational Aerodynamics of Hovering Helicopter Rotors. Jurnal Mekanikal. 34: 16-46.

[6] Gagliardi A. and Barakos, G.N. 2009. Analysis and Design of a Flapped-Equipped Low-Twist Rotor for Hover. Journal of Aircraft. 46(1): 74-84.

[7] M. Bilgili, A. Yasar, A. Ilhan, B. Sahin. 2015. Aerodynamic Characteristics of a Horizontal Axis Wind Turbine in Belen-Hatay, Turkey. International journal of Natural and Engineeing Science. 9(1): 54-58.

[8] Kishinami K, Taniguchi H, Suzuki J, Ibano H, Kazunou T, Turuhami M. 2005. Theoretical and experimental study on the aerodynamic characteristics of a horizontal axis wind turbine, Energy. 2005: 2089-2100.

[9] R. Steijl, F. Dehaeze, G.N. Barakos, L.I. Garipova, A.N. Kusyumov, S. A. Mikhailov. 2015. Simulation of Flow around Blade Section with One Degree of Freedom Aeroelastic Flap4. Russian Aeronautics (Iz.VUZ). 58(2): 193-198.

[10] Riadh W.Y. Habash, Voicu Groza, Yue Yang, Charles Blouin, Pierre Guillemette. 2011. Performance of a Contrarotating Small Wind Energy Converter. International Scholarly Research Network ISRN Mechanical Engineering. 2011: 1-10.

[11] Jang-Oh Mo, Young-Ho Lee. 2012. CFD Investigation on the aerodynamic characteristics of a small-sized wind turbine of NREL PHASE VI operating with a stall-regulated method. Journal of Mechanical Science and Technology. 26(1): 81-92.

[12] N.N. Sorensen, J.A. Michelsen. 2000. Aerodynamic predictions for the unsteady aerodynamics experiment Phase II rotor at the national renewable energy laboratory, AIAA Paper, 2000-0037.

[13] D. Simms, S. Schreck, M. Hand and L. J. Fingersh. 2001. NREL Unsteady aerodynamics experiment in the NASA-Ames wind tunnel: A Comparison of predictions to measurements, National Renewable Energy Laboratory, NREL/TP-500-29494.

[14] Nurimbetov A.U., Orynbayev S.A., Junisbekov M. Sh., Omarov Zh.T. 2019. Numerical Solution Stressed Defressed Condition of Multilayer Composition Blades in the Field of Centrifugal Forces. News of NAS RK. Series of Geology and Technical Sciences. 5(437): 60-73.

[15] Nurimbetov A., Bekbayev A., Orynbayev S., Dzhamanbayev M., Keikimanova M. 2015. Naturally Twisted Layered Anisotropic Rod Made of Reinforced Materials Research. Applied Mechanics and Materials. 736: 30-38.